A Discrete Constraint for Entropy Conservation and Sound Waves in Cloud-Resolving Modeling

Xiping Zeng

Goddard Earth Sciences and Technology Center, University of Maryland, Baltimore County, and Laboratory for Atmospheres, NASA Goddard Space Flight Center, Greenbelt, Maryland

Wei-Kuo Tao and **Joanne Simpson**

Laboratory for Atmospheres, NASA Goddard Space Flight Center, Greenbelt, Maryland

Popular Summary

Ideal cloud-resolving models contain so little accumulative errors that they can simulate cumulus clouds and synoptic large-scale circulations correctly. This paper discusses a discrete constraint for the models in relation to no accumulative errors or the correct representation of the large-scale convergence and advection of scalars (e.g. moist entropy, water vapor). The paper further shows that the challenge is how to compute sound waves efficiently under the constraint.

To address the challenge, the paper proposes a compensation method for the efficient computation of sound waves. Stability analysis and numerical experiments show that the method allows the models to integrate efficiently with a large time step.

In contrast to the time-split method, the compensation method needs no small-time-step integration for sound waves. As a result, the method is slightly more efficient than the time-split method when one processor is used, and much more efficient when many (e.g., hundreds of) processors are used for cloud-resolving modeling.

A Discrete Constraint for Entropy Conservation and Sound Waves in Cloud-Resolving Modeling

Xiping Zeng

Goddard Earth Sciences and Technology Center, University of Maryland, Baltimore County, and Laboratory for Atmospheres, NASA Goddard Space Flight Center, Greenbelt, Maryland

Wei-Kuo Tao and Joanne Simpson

Laboratory for Atmospheres, NASA Goddard Space Flight Center, Greenbelt, Maryland

January 15, 2003

Submitted to *Journal of the Atmospheric Sciences*

Abstract

Ideal cloud-resolving models contain little accumulative errors. When their domain is so large that synoptic large-scale circulations are accommodated, they can be used for the simulation of the interaction between convective clouds and the large-scale circulations. This paper sets up a framework for the models, using moist entropy as a prognostic variable and employing conservative numerical schemes. The models possess no accumulative errors of thermodynamic variables when they comply with a discrete constraint on entropy conservation and sound waves. Alternatively speaking, the discrete constraint is related to the correct representation of the large-scale convergence and advection of moist entropy.

Since air density is involved in entropy conservation and sound waves, the challenge is how to compute sound waves efficiently under the constraint. To address the challenge, a compensation method is introduced on the basis of a reference isothermal atmosphere whose governing equations are solved analytically. Stability analysis and numerical experiments show that the method allows the models to integrate efficiently with a large time step.

1. Introduction

Massive parallel computation upgrades the environment for atmospheric modeling by domain decomposition (e.g., Droegemeier *et al.* 1995, Juang *et al.* 2003), breeding the next generation of cloud-resolving models (e.g., a global cloud-resolving model). The future models will take so large a domain that they simulate both convective clouds and large-scale circulations explicitly, addressing the interaction among clouds, radiation and large-scale circulations. In contrast to current cloud-resolving models, the future models will possess little accumulative errors for the correct simulation of large-scale circulations.

Large-scale circulations are governed by thermodynamics in the Tropics (Raymond 1995, 2000; Raymond and Zeng 2000; Zeng, Tao and Simpson 2004). Zeng, Tao and Simpson (2004) used the analytical model of Neelin and Held (1987) to show the sensitivity of tropical large-scale vertical circulations to atmospheric cooling rate. Their results indicated that, for the correct simulation of tropical large-scale vertical circulations, the accumulative temperature error should be much less than 1 K/day, the order of the atmospheric radiative cooling rate. In other words, the accumulative temperature error should be ~10^{-1} K/day or less for the simulation of large-scale circulations.

On the basis of the scale analysis of atmospheric convection (Ogura and Phillips 1962), the current cloud-resolving models were constructed to simulate individual cloud systems for life-cycle characteristics (e.g., Klemp and Wilhelmson 1978, Grabowski 1989, Tao and Simpson 1993, Tompkins and Craig 1998, Xue *et al.* 2000, Tao *et al.* 2003). Some small terms were usually ignored for economical computation, which may distort the simulation of large-scale circulations. For example, the sink of moist air was ignored in expressing the air mass continuity equation in terms of the

density of moist air. The approximation of no moist air sink can bring about an accumulative temperature error of 10^{-1} K/day with a large-scale vertical velocity of 1 cm/s (see Appendix A). Although such error can be ignored in the simulation of individual cloud systems for life-cycle characteristics, it can distort the simulation of tropical large-scale circulations.

Moreover, numerical errors can distort the simulation of large-scale circulations. The current cloud-resolving models usually employ temperature (or its equivalent) as a prognostic thermodynamic variable. They compute sound waves economically with some approximations. If the approximations violate energy conservation, the accumulative temperature error may not be less than 10^{-1} K/day. Consider a cloud-resolving model with a 10-second time step and a random temperature error around 10^{-1} K in one integration step. When the random error is averaged over many grid points and time levels, its value can exceed 10^{-5} K statistically in many cases, where the error of 10^{-5} K per step corresponds to an accumulative temperature error of 10^{-1} K/day. Hence, large numerical errors can sometimes distort the simulation of large-scale circulations.

The new trend is to replace temperature with moist entropy as a prognostic variable and diagnose the temperature from that and other prognostic variables (Raymond and Blyth 1986; Ooyama 1990, 2001; Zeng 2001; Zeng, Tao and Simpson 2004). Moist entropy deals "easily" with the transition between the three water phases. If it is used as a prognostic variable, it can reduce numerical errors especially those connected with microphysical and dynamic processes (Zeng 2001; Zeng, Tao and Simpson 2004). Recently, Ooyama (2001) and Zeng (2001) constructed two- and three-dimensional models with moist entropy as a prognostic variable, respectively, to simulate warm clouds. Zeng, Tao and Simpson (2004) derived an accurate equation

for moist entropy, providing a theoretical basis for using moist entropy as a prognostic variable in long-term cloud modeling. Hence, one possible framework for the simulation of the large-scale circulation is a cloud-resolving model with moist entropy as a prognostic variable.

If a cloud-resolving model uses moist entropy as a prognostic variable and discretizes the moist entropy and other prognostic thermodynamic variables in conservative forms, it contains no accumulative error of the prognostic thermodynamic variables. Since temperature is diagnosed from the moist entropy and the other prognostic thermodynamic variables, the model contains no accumulative temperature error either. However, the conservative discrete form of the moist entropy involves air density, and the air density is related to sound waves through the air mass continuity equation. Although sound waves are meteorologically unimportant, their phase speed limits the time step for integration. Thus, the challenge is how to compute sound waves economically while conserving moist entropy (see Section 2 for more discussion).

Many good numerical schemes for sound waves have been proposed for life-cycle modeling of individual cloud systems (e.g., Klemp and Wilhelmson 1978, Anderson, *et al.* 1985, Droegemeier and Wilhelmson 1987, Skamarock and Klemp 1992) and long-term cloud ensemble modeling (Zeng 2001, Satoh 2002). However, those schemes do not suit the cloud-resolving model well for the simulation of large-scale circulations, because the model is expected to possess the following three characteristics: (1) efficient computation with a single processor and highly efficient massive parallel computation with 10^2-10^3 processors, (2) entropy or energy conservation, and (3) no accumulative error even from the computation of sound waves. To prepare such models for the simulation of large-scale circulations, this

paper introduces an efficient method for computing sound waves on the basis of a reference atmosphere whose governing equations are solved analytically.

With the explicit simulation of convective clouds and large-scale circulations as the background, this paper proposes a framework for future cloud-resolving models and deals with the computation of sound waves in the framework. The paper consists of five sections. Section 2 introduces a framework for cloud-resolving models with moist entropy as a prognostic variable. It explains a discrete constraint on entropy conservation and sound waves that corresponds to no accumulative error of thermodynamic variables. Section 3 develops an efficient method to compute sound waves, and Section 4 tests the method with numerical experiments. Section 5 gives a summary.

2. Entropy conservation and sound waves

Accumulative errors in a numerical model originate in the continuous governing equations and their discretization. When the air mass continuity equation is expressed in the density of moist air and the sink of moist air due to water vapor condensation is ignored, there is an accumulative temperature error in the continuous governing equations. The error, as shown in Appendix A, is so large that it sometimes can distort the simulation of tropical, large-scale circulations. To remove the error and similar others, a framework for cloud-resolving models is set up for the simulation of large-scale circulations.

a. A framework for cloud-resolving models

A framework is set up for cloud-resolving models with no accumulative error of thermodynamic variables, where the density of dry air and the moist entropy are used

as prognostic variables. Specifically speaking, the density of *dry* air ρ is used to rewrite the ideal gas law, the air mass continuity equation and the flux form of prognostic thermodynamic variables.

The ideal gas law for moist air is written as

$$p = \rho R_d T(1+1.608q_v) \tag{2.1}$$

where p is the total pressure of moist air, T the air temperature, q_v the mixing ratio of water vapor and R_d the gas constant of dry air.

The momentum equation for moist air (including precipitating particles) is written as

$$\partial_t \mathbf{v} + \rho \mathbf{q} \times \mathbf{v} + \nabla K = -\frac{1}{\rho(1+q_t+q_p)}\nabla p + \mathbf{g} + \mathbf{D}_v \tag{2.2}$$

where $\mathbf{v}$ is the velocity vector and $\mathbf{g}$ the acceleration due to gravity; $\mathbf{D}_v$ represents the subgrid diffusion of momentum due to turbulence; $K \equiv \frac{1}{2}\mathbf{v}\cdot\mathbf{v}$ is the kinetic energy per unit mass; $\mathbf{q} \equiv \rho^{-1}(\nabla \times \mathbf{v} + 2\Omega)$ is the vorticity divided by air density where $\mathbf{\Omega}$ is the angular velocity vector of the Earth's rotation; q_t is the total mixing ratio of airborne water and q_p the mixing ratio of precipitating particles. If q_c, q_i, q_r, q_s and q_g denote the mixing ratios of cloud water, cloud ice, rainwater, snow and grauple/hail, respectively, the total mixing ratios of airborne water and precipitating particles are expressed as

$$q_t = q_v + q_c + q_i$$

$$q_p = q_r + q_s + q_g$$

The mass continuity equation for dry air is

$$\partial_t \rho + \nabla \cdot (\rho \mathbf{v}) = 0 \tag{2.3}$$

and the prognostic equation for a scalar ϕ is

$$\partial_t \rho\phi + \nabla \cdot (\rho \mathbf{v} \phi) = \rho(M_\phi + D_\phi) \tag{2.4}$$

where M_ϕ refers to the microphysical processes in clouds and D_ϕ the scalar subgrid mixing due to turbulent eddies.

The symbol ϕ in Equation (2.4) represents s the moist entropy, q_l, q_i, q_r, q_s and q_g the mixing ratios of airborne water, cloud ice, rainwater, snow and graupel/hail. Following the notation of Tao and Simpson (1993), the microphysical processes are described by M_ϕ (ϕ=s, q_l , q_i, q_r, q_s and q_g) or

$$M_{qt} = E_r + S_s + S_g - (T_{qc} + T_{qi}) \tag{2.5a}$$

$$M_{qi} = -S_i - T_{qi} \tag{2.5b}$$

$$M_{qr} = \rho^{-1} \partial_z (\rho V_{tr} q_r) - E_r - F_s - F_g - T_{qr} \tag{2.5c}$$

$$M_{qs} = \rho^{-1} \partial_z (\rho V_{ts} q_s) - S_s + F_s - T_{qs} \tag{2.5d}$$

$$M_{qg} = \rho^{-1} \partial_z (\rho V_{tg} q_g) - S_g + F_g - T_{qg} \tag{2.5e}$$

$$M_s = G_s + (Q - \mathbf{v} \cdot \mathbf{D}_\mathbf{v})/T \tag{2.5f}$$

where V_t is the terminal velocity of precipitating particles; E, F and S stand for evaporation, fusion/freezing and sublimation/deposition, respectively; and T_{qc}, T_{qr}, T_{qi}, T_{qs}, and T_{qg} represent the microphysical transfer rates between hydrometeor species and their sum is zero.

In Equation (2.5f), Q is the rate of diabatic heating and G_s the internal source of moist entropy; the term $-\mathbf{v}\cdot\mathbf{D}_\mathbf{v}$ represents the heat generated by internal friction and is introduced for energy conservation. The moist entropy s is defined in unit mass of dry air, representing the contribution from dry air, water vapor, cloud water and ice except for precipitating particles. The complete flux-form equation for moist entropy was introduced by Zeng, Tao and Simpson (2004). In other words, the expression for G_s is known.

The models employ the following prognostic variables: the velocity vector **v**, the air density ρ, the moist entropy s, the total mixing ratio of airborne water q_t, the mixing ratio of cloud ice q_i, and the mixing ratios of rainwater q_r, snow q_s and graupel/hail q_g. Their corresponding prognostic equations are Equations (2.2), (2.3) and (2.4). Once the prognostic variables are known, the total pressure of moist air p is determined by Equation (2.1), and the quantities T, q_v and q_c are diagnosed from the prognostic variables s, q_t and q_i.

b. A discrete constraint

Scalars are conserved in advection, to which the intension of "conservation" is confined in this paper. It is easy to apply conservative schemes to Equations (2.3) and (2.4). When the scalar ϕ is constant and $M_\phi = D_\phi = 0$, the discrete form of Equation (2.4) should reduce into that of Equation (2.3), which is referred to here as a discrete constraint. Recently the constraint has attracted attention because of its importance in the construction of a model for the interaction between tropical convection and large-scale circulations (Zeng 2001, Arakawa 2004). Zeng (2001) constructed a three-dimensional cloud-resolving model under the constraint to simulate tropical convective clouds and their interaction with large-scale circulations. Arakawa (2004) referred to the constraint as "constancy" warranty and related the constraint to the correct representation of the advection and convergence of scalars such as water vapor.

When the models in the preceding subsection employ conservative schemes, the constraint corresponds to no accumulative error of thermodynamic variables. In the models without the constraint, accumulative errors exist, one of which on ϕ is understood from the following mathematical operations. Substituting ϕ in the discrete

form of Equation (2.4) with $\phi+\phi_c$, then subtracting the discrete form of Equation (2.3) times ϕ_c yields a resulting equation, where the constant ϕ_c is chosen arbitrarily. In comparison with the discrete form of Equation (2.4), the resulting equation contains a new string that is composed of all terms with ϕ_c. The new string represents an error and is proportional to ϕ_c. When the error is accumulated, the simulation of large-scale circulations may be distorted[1].

In fact, it is easy to discretize Equations (2.3) and (2.4) under the constraint. A key question is how to compute sound waves efficiently under the constraint. Since the discrete form of Equation (2.3) is related to sound waves through the ideal gas law, the speed of sound waves limits the time step for integration. To construct an efficient scheme for sound waves, the ideal gas law or Equation (2.1) is modified to

$$\frac{\partial p}{\partial t} = p\left(\frac{\partial \rho}{\rho \partial t} + \frac{\partial T}{T \partial t} + \frac{1.608}{1+1.608q_v}\frac{\partial q_v}{\partial t}\right) - \frac{p - \rho R_d T(1+1.608q_v)}{\tau_s} \qquad (2.6)$$

where the relaxation timescale τ_s is chosen to be 5 minutes or so.

Equation (2.6) is close to the ideal gas law. Once it deviates from the ideal gas law as it sometimes can due to computational reasons, it soon relaxes to the ideal gas law on the timescale τ_s. Its temporary deviation from the ideal gas law provides room for

[1] For a given numerical scheme, the error is estimated as follows. Assume that ϕ is constant. Dividing the discrete form of Equation (2.4) by ϕ, then subtracting the discrete form of Equation (2.3), and finally moving all terms to the right side yields a resulting equation. The right side equals zero under the constraint. Otherwise, the right side represents a spurious mass sink in a discrete equation for either air mass continuity or scalar advection. The spurious mass sink is compared with the sink of moist air due to water vapor condensation, estimating the order of the error just as doing in Appendix A.

the numerical treatment of sound waves under the constraint and brings about no accumulative error of thermodynamic variables.

3. A compensation method for sound waves

An efficient method is introduced in this section to compute sound waves under the constraint. For simplicity, the method is illustrated in a one-dimensional dry model as an example without loss of generality. From Equations (2.2), (2.3) and (2.6), the equations for a one-dimensional dry atmosphere are written as

$$\partial_t \rho w + \partial_z p + \rho g + \cdots = 0 \tag{3.1a}$$

$$\partial_t \rho + \partial_z \rho w + \cdots = 0 \tag{3.1b}$$

$$\partial_t p - R_d T \partial_t \rho + (p - \rho R_d T)\tau_s^{-1} + \cdots = 0 \tag{3.1c}$$

where z is the height and w the vertical velocity component; and the temperature T is fixed for the convenience of description.

In contrast to Equation (3.1), a simple reference isothermal atmosphere is introduced with the following governing equations

$$\partial_t \rho w + \partial_z p + \rho g = 0 \tag{3.2a}$$

$$\partial_t \rho + \partial_z \rho w = 0 \tag{3.2b}$$

$$\partial_t p - R_d T_{ref} \partial_t \rho = 0 \tag{3.2c}$$

where the temperature T_{ref} is a constant. Subtracting the left sides of Equation (3.2) from both sides of Equation (3.1) yields

$$\begin{aligned} &\left(\partial_t \rho w + \partial_z p + \rho g + \cdots\right) \\ &-\left(\partial_t (\rho w)^{(d)} + \partial_z p^{(d)} + \rho g\right) = -\left(\partial_t (\rho w)^{(a)} + \partial_z p^{(a)} + \rho g\right) \end{aligned} \tag{3.3a}$$

$$\begin{aligned} &\left(\partial_t \rho + \partial_z \rho w + \cdots\right) \\ &-\left(\partial_t \rho^{(d)} + \partial_z (\rho w)^{(d)}\right) = -\left(\partial_t \rho^{(a)} + \partial_z (\rho w)^{(a)}\right) \end{aligned} \tag{3.3b}$$

$$\begin{aligned}&\left(\partial_t p - R_d T \partial_t \rho + (p - \rho R_d T)\tau_s^{-1} + \cdots\right)\\ &-\left(\partial_t p^{(d)} - R_d T_{ref} \partial_t \rho^{(d)}\right) = -\left(\partial_t p^{(a)} - R_d T_{ref} \partial_t \rho^{(a)}\right)\end{aligned} \tag{3.3c}$$

where the superscripts (d) and (a) are introduced only to group terms for different numerical schemes. Strictly speaking, Equation (3.3) is equivalent to Equation (3.1) because a variable with the superscript (d) represents the same property of the real atmosphere as its corresponding variable with the superscript (a). Hence

$$\partial_t \rho w = \partial_t (\rho w)^{(d)} = \partial_t (\rho w)^{(a)} \tag{3.4a}$$

$$\partial_t \rho = \partial_t \rho^{(d)} = \partial_t \rho^{(a)} \tag{3.4b}$$

$$\partial_t p = \partial_t p^{(d)} = \partial_t p^{(a)} \tag{3.4c}$$

a. Symbol notation

Equations (3.1), (3.2) and (3.3) are discretized on three time levels, from the time level n–1 to n+1, and four sets of symbols are introduced for concise expressions. Any variable for a given property in the three equations takes the same values on the time levels n-1 and n except for on the time level n+1. The symbols ($w^{(n+1)}$, $\rho^{(n+1)}$, $p^{(n+1)}$) denote the final values of variables on the time level n+1 in the numerical method, and (w^*, ρ^*, p^*) the values on the time level n+1 that are calculated from the finite-difference form of Equation (3.1). If ($w^{(n+1)}$, $\rho^{(n+1)}$, $p^{(n+1)}$)= (w^*, ρ^*, p^*) is set, the time step for integration is limited by the speed of sound waves, which degenerates into a traditional method.

The symbols ($w^{(d)}$, $\rho^{(d)}$, $p^{(d)}$) and ($w^{(a)}$, $\rho^{(a)}$, $p^{(a)}$) denote the two sets of variables on the time level n+1. They are calculated numerically from the finite-difference form of Equation (3.2) and analytically from Equation (3.2), respectively. Because ($w^{(d)}$, $\rho^{(d)}$, $p^{(d)}$) and ($w^{(a)}$, $\rho^{(a)}$, $p^{(a)}$) approximate the same properties of the reference atmosphere

in two different ways[2], their difference is close to zero theoretically. Thus the values $(w^*-w^{(d)}+w^{(a)}, \rho^*-\rho^{(d)}+\rho^{(a)}, p^*-p^{(d)}+p^{(a)})$ still approximate the solution of Equation (3.1) or (3.3) on the time level $n+1$. In other words, $(w^{(a)}-w^{(d)}, \rho^{(a)}-\rho^{(d)}, p^{(a)}-p^{(d)})$ compensate (w^*, ρ^*, p^*) for the final values, which increases the maximum time step for stable integration and is referred to here as the compensation method.

The four sets of symbols are illustrated in the preceding paragraphs. Next is the computational procedure in the compensation method with *accurate* definitions of the symbols. Apply similar finite-difference schemes to Equations (3.1) and (3.2), and use their discrete forms to calculate (w^*, ρ^*, p^*) and $(w^{(d)}, \rho^{(d)}, p^{(d)})$ on the time level $n+1$, respectively. Then introduce the symbols

$$S_{cw} = ((\rho w)^{*n+1} - (\rho w)^{(d)n+1})/2\Delta t \tag{3.5a}$$

$$S_{c\rho} = (\rho^{*n+1} - \rho^{(d)n+1})/2\Delta t \tag{3.5b}$$

$$S_{cp} = (p^{*n+1} - p^{(d)n+1})/2\Delta t \tag{3.5c}$$

where Δt is the time step and the superscript $n+1$ is added to distinguish the variables on the time level $n+1$ from the variables on other time levels. Using Equations (3.4) and (3.5), Equation (3.3) is rewritten as

$$\partial_t(\rho w)^{(a)} + \partial_z p^{(a)} + \rho^n g = S_{cw} \tag{3.6a}$$

$$\partial_t \rho^{(a)} + \partial_z(\rho w)^{(a)} = S_{c\rho} \tag{3.6b}$$

$$\partial_t p^{(a)} - R_d T_{ref} \partial_t \rho^{(a)} = S_{cp} \tag{3.6c}$$

[2] The symbols $(w^{(d)}, \rho^{(d)}, p^{(d)})$ and $(w^{(a)}, \rho^{(a)}, p^{(a)})$ refer to the reference atmosphere only in this paragraph for easy understanding. They are defined accurately in the following paragraphs. In fact, it is unnecessary for a mathematician to introduce the reference atmosphere because the method does not need an equation like Equation (3.2).

with the initial condition

$$(\rho w)^{(a)} = \rho^{n-1} w^{n-1} \tag{3.6e}$$

$$p^{(a)} = p^{n-1} \tag{3.6f}$$

at $t=(n\text{-}1)\Delta t$ and the boundary condition

$$(\rho w)^{(a)} = \rho_1^{n-1} w_1^{n-1} \qquad \text{at } z=0 \tag{3.6g}$$

$$(\rho w)^{(a)} = 0 \qquad \text{at } z=z_{top}, \tag{3.6h}$$

where z_{top} is the height of the top boundary, and the variables with the subscript "1" refer to the properties near the surface.

Equation (3.6) is solved analytically for ($w^{(a)n+1}$, $\rho^{(a)n+1}$, $p^{(a)n+1}$) the values at $t=(n+1)\Delta t$. From this and Equation (3.4) the final solution of Equation (3.1) at the time level $n+1$ is obtained. That is

$$w^{n+1}=w^{(a)n+1} \tag{3.7a}$$

$$\rho^{n+1}=\rho^{(a)n+1} \tag{3.7b}$$

$$p^{n+1}=p^{(a)n+1} \tag{3.7c}$$

b. Solution expression

This subsection shows how to solve Equation (3.6) analytically. Let $c_{sr}=(R_d T_{ref})^{1/2}$ denote the sound wave speed in the reference atmosphere and $z_s=2c_{sr}\Delta t$ the distance that the sound waves travel in $2\Delta t$. Assume that S_{cw}, $S_{c\rho}$ and S_{cp} do not change with time between the time levels $n-1$ and $n+1$. From the boundary condition of Equation (3.6), w and p are set as

$$\begin{aligned}(\rho w)^{(a)n+1} &= W' + \rho_1^{n-1} w_1^{n-1}(1 - z/z_{top}) + \tfrac{1}{2} c_{sr}^{-1} \int_{z-z_s}^{z+z_s} S_{cw}(z)dz \\ &- \tfrac{1}{2}\int_{z}^{z+z_s} \left(c_{sr}^{-2} S_{cp}(z) + S_{c\rho}(z)\right)dz + \tfrac{1}{2}\int_{z-z_s}^{z} \left(c_{sr}^{-2} S_{cp}(z) + S_{c\rho}(z)\right)dz\end{aligned} \tag{3.8a}$$

$$p^{(a)n+1} = p' + 2\Delta t c_{sr}^2 \rho_1^{n-1} w_1^{n-1} / z_{top} + p_s^n - g\int_o^z \rho^n dz$$
$$+\tfrac{1}{2} c_{sr}^{-1} \int_{z-z_s}^{z+z_s} \left(S_{cp}(z) + c_{sr}^2 S_{c\rho}(z)\right) dz - \tfrac{1}{2}\int_z^{z+z_s} S_{cw}(z)dz + \tfrac{1}{2}\int_{z-z_s}^{z} S_{cw}(z)dz \quad (3.8b)$$

where p_s is the surface pressure; and the new variables $W'(z, t)$ and $p'(z, t)$ satisfy

$$\partial_t W'(z,t) + \partial_z p'(z,t) = 0 \quad (3.9a)$$

$$\partial_t p'(z,t) + c_{sr}^2 \partial_z W'(z,t) = 0 \quad (3.9b)$$

with the boundary conditions $W'(z, t)=0$ at $z=0$ and z_{top}, and the initial conditions

$$W'(z,t) = W_0(z) \equiv \rho^{n-1} w^{n-1} - \rho_1^{n-1} w_1^{n-1}(1 - z / z_{top}) \quad (3.9c)$$

$$p'(z,t) = p_0(z) \equiv p^{n-1} - p_s^n + g\int_0^z \rho^n dz \quad (3.9d)$$

at $t=(n\text{-}1)\Delta t$. Equation (3.9) is solved analytically, giving

$$W' = \frac{W_0(z+z_s) + W_0(z-z_s)}{2} - \frac{p_0(z+z_s) - p_0(z-z_s)}{2c_{sr}} \quad (3.10a)$$

$$p' = \frac{p_0(z+z_s) + p_0(z-z_s)}{2} - c_{sr}\frac{W_0(z+z_s) - W_0(z-z_s)}{2} \quad (3.10b)$$

at $t=(n+1)\Delta t$, where the function W_0 and p_0 are extended to $(-\infty,+\infty)$ with their symmetry to $z=0$ and z_{top}.

To calculate w and p on the time level $n+1$ with Equations (3.8) and (3.10), the values of w and p on the time level n-1 between grid points are needed. They are calculated by linear interpolation. As a side effect of the linear interpolation, sound waves are damped.

The air density ρ^{n+1} is calculated with Equation (3.6c) after the pressure p^{n+1} is known. Since the pressure p^{n+1} is calculated with the aid of linear interpolation, the vertical integration of ρ^{n+1}-$\rho^{*\,n+1}$ may not equal zero. For mass conservation, a slight adjustment of ρ^{n+1} is taken so that the vertical integration of ρ^{n+1}-$\rho^{*\,n+1}$ equals zero.

c. Stability explanation

The numerical stability of the compensation method is analyzed in Appendix B for a linear system that is close to the preceding one. Here is a physical explanation for the numerical stability. The method, as Equations (3.3) and (3.6) show, works like two systems. The two systems step forward in turn. One system is governed by Equation (3.3) with zeros on its right sides. Its sound wave speed $(R_d(T-T_{ref}))^{1/2}$ is low. It is simulated with finite-difference schemes. Its time step is limited by the low sound wave speed if no other system is involved.

The other system is governed by Equation (3.6). Its sound wave speed $(R_d T_{ref})^{1/2}$ is high. The system is simulated with analytical schemes instead of finite-difference schemes. Thus the time step for integration is not limited by the high sound wave speed.

The two systems step forward in turn. First the slow "sound waves" propagate locally. Then their residue is carried by the fast "sound waves" into a vast space. As a result, the "sound waves" accomplish the adjustment between the velocity and the pressure fields in the models even though the "sound waves" do not imitate real sound waves well. Since the time step for integration is not limited by the high sound wave speed, the models can be integrated with a large time step. The maximum time step for stable integration can be determined by the Fourier stability analysis such as in Appendix B or the numerical tests in the next section.

4. Numerical tests

To test the compensation method, a one-dimensional atmosphere that is governed by Equation (3.1) without ellipses is chosen as a test case. Initially the atmosphere is stationary and in hydrostatic equilibrium; the surface pressure is 1013.25 hpa; the

temperature decreases linearly with height from the surface value of 288 to 216.5 K at z=11 km and remains constant above 11 km. The atmospheric rigid boundaries are located at z=0 and z_{top}=18 km. A vertical force

$$F_c = 10^{-2}\, g \sin(\frac{\pi t}{\tau_c}) \sin(\frac{3\pi z}{2z_{top}}) \qquad \text{when } z<2z_{top}/3$$

is applied to a unit mass of air, where the timescale τ_c=40 minutes. The force, imitating the buoyancy in convective cells with updrafts and downdrafts in turn, drives the atmospheric motion.

Two experiments with a vertical grid size Δz=600 m are done to simulate the atmosphere, using the compensation method and the traditional method in Appendix B, respectively. A time-smoother (Robert 1966) is used to remove any tendencies that might decouple the odd and even steps. In the experiment with the traditional method, the time step Δt=0.1 seconds although the maximum time step for stable integration is close to 1 second. Since the time step is so small, the results in the experiment are treated as a standard benchmark to measure the results in the other experiment. One result in the experiment, the vertical velocity $\rho w/\rho_s$ at z=6 km with ρ_s=1 kg/m^3 versus time, is displayed in the upper panel of Figure 1, showing the superimposition of the oscillations of sound waves on a forced oscillation.

In the experiment with the compensation method, the time step Δt=10 seconds, the reference temperature T_{ref}=273.15 K, and the relaxation timescale τ_s=5 minutes. The vertical velocity at z=6 km versus time is displayed in the lower panel of Figure 1. In contrast to the results in the experiment with the traditional method, the forced motion due to buoyancy is simulated well although the sound waves are not simulated well.

The two experiments are re-done to show why the sound waves are not simulated well in the compensation method. In the two new experiments, a sponge layer is

introduced above 15 km to absorb sound waves. The maximum time scale for damping sound waves is 30 seconds at the top boundary. Figure 2 displays the same variable in Figure 1 for the new experiments. As the figure shows, the forced oscillations in the two experiments are similar. In the traditional method, the force generates sound waves and the sound waves are damped in the sponge layer. In contrast, in the compensation method, not only the force but also the numerical schemes generate sound waves. The sound waves are damped not only in the sponge layer but also by the numerical schemes. Based on Figure 1, the sound waves are mainly damped by the numerical schemes. Otherwise, the amplitude of sound wave fluctuation would increase with time.

Since the numerical schemes in the compensation method generate sound waves continuously as computational noise, an interesting question is whether the noise affects the simulation of meteorological phenomena. If the numerical scheme for scalar advection in Appendix C is used corresponding with the compensation method, sound waves bring about no accumulative error of thermodynamic variables. As a result, sound waves do not affect meteorological motion.

Two experiments are conducted to show that sound waves do not affect meteorological motion. In one of them, the traditional method with a small time step (Δt=0.1 s) is used, and a sponge layer for sound waves is introduced. Results for the first five hours are shown in the upper panel of Figure 2, and the results after 70 days are shown by the thick line in Figure 3. Since sound waves are damped completely in 70 days, the thick line represents the meteorological motion. In the other experiment, the compensation method with a large time step (Δt=10 s) is used, and there is no sponge layer for sound waves. Results for the first five hours are shown in the lower panel of Figure 1, and the results after 70 days are shown by the thin line in Figure 3.

Figure 3 clearly shows that the compensation method simulates the meteorological motion quite well in the long-term integration in the presence of computational sound waves.

5. Discussion and summary

On the basis of the scale analysis of atmospheric convection (Ogura and Phillips 1962), almost all current cloud-resolving models ignored some small terms for economical computation. Those models have successfully simulated convective cloud systems for life-cycle characteristics. When they are extended to the simulation of large-scale circulations, however, the question is whether the small terms are still ignorable.

Zeng, Tao and Simpson (2004) used the analytical model of Neelin and Held (1987) to diagnose large-scale vertical velocity in the Tropics. Their results showed the sensitivity of large-scale vertical circulations to the atmospheric cooling rate and the surface flux of moist entropy from the underlying surface to the air above. Since the atmospheric radiative cooling rate is 1 K/day or so, their results indicate that the accumulative temperature error should be equal to 10^{-1} K/day or less for the simulation of tropical large-scale vertical circulations.

Using the value of 10^{-1} K/day as a scale, the approximations in the current cloud-resolving models are re-checked for the simulation of large-scale circulations. It is found that some approximations should be removed. For example, the density of moist air should be replaced with the density of dry air in expressing the air mass continuity equation (see Appendix A), and the thermal capacity of precipitating particles should be taken into account (Zeng, Tao and Simpson 2004). A discrete

constraint on the consistency between the discrete scalar equation and the discrete air mass continuity equation should be addressed.

For the correct simulation of large-scale circulations, a framework is set up for cloud-resolving models that use the density of dry air to express the air mass continuity equation and employ moist entropy as a prognostic variable. In the models, the flux-form equation for moist entropy takes account of the thermal capacity of precipitating particles (Zeng, Tao and Simpson 2004).

The models possess no accumulative error of thermodynamic variables when they comply with a discrete constraint on entropy conservation and sound waves. The constraint requires that the discrete flux-form equation for scalar advection reduce into the discrete equation for air mass continuity while the scalar is constant. Since air density is involved in the flux-form equation for scalar advection and is related to sound waves through the air mass continuity equation, the challenge is how to compute sound waves efficiently under the constraint.

To address the challenge, a compensation method is developed for the efficient computation of sound waves, where a reference isothermal atmosphere is introduced. The governing equations for the reference atmosphere are solved both analytically and numerically. The difference between the analytical and the numerical solutions is used to compensate the original solution of the models with traditional finite-difference schemes. Once the original solution is compensated, the models simulate sound waves equivalently by "analytical" schemes rather than finite-difference schemes (see the text for an accurate description). As a result, the time step for integration is not limited by the high speed of sound waves, and the models can integrate efficiently with a large time step.

The compensation method for sound waves is tested in a one-dimensional model. Numerical experiments show that the method with a large time step is stable and can simulate meteorological motions quite well in a long-term integration. On the same principle, the method can be extended to multi-dimensional models easily. The compensation method in a three-dimensional, terrain-following coordinate system is technically complicated and will be introduced elsewhere as a technical report.

In contrast to the time-split method (Klemp and Wilhelmson 1978), the compensation method needs no small-time-step integration for sound waves. Thus, when one processor is used for computation, the models with the compensation method run slightly faster than those with the time-split method. Recent parallel computation tests of the Goddard Cumulus Ensemble model (Tao *et al.* 2003) on memory-distributed machines showed that the efficiency of parallel computation is degraded by the data communication between processors in computing sound waves, especially while hundreds of processors are used. Without small-time-step integration for sound waves, the compensation method is expected to be much more efficient than the time-split method in massive parallel computation for cloud-resolving modeling.

Acknowledgements. The work is supported by the NASA Headquarters Atmospheric Dynamics and Thermodynamics Program and the NASA Tropical Rainfall Measuring Mission (TRMM). The authors are grateful to Dr. R. Kakar at NASA headquarters for his support of this research. The authors also thank Mr. S. Lang for reading the manuscript.

APPENDIX A

Analysis of Accumulative Temperature Error

In this appendix, the temperature error is analyzed in a set of continuous governing equations, one of which, the air mass continuity equation, ignores the sink of moist air due to water vapor condensation or deposition. To show the error, the density of moist air ρ_t is distinguished from the density of dry air ρ_d by $\rho_t = \rho_d(1+q_v)$. Differentiating the proceeding relation yields

$$d\ln\rho_t / dt \approx d\ln\rho_d / dt + dq_v / dt \tag{A1}$$

If the potential temperature θ is described by $d\theta/dt = M_\theta$ where M_θ represents the source of potential temperature, the accurate flux form of θ is

$$\frac{\partial \rho_d \theta}{\partial t} + \nabla\cdot(\rho_d \theta \mathbf{v}) = \rho_d M_\theta \tag{A2}$$

When a cloud-resolving model uses the following prognostic equation

$$\frac{\partial \rho_t \theta}{\partial t} + \nabla\cdot(\rho_t \theta \mathbf{v}) = \rho_t M_\theta \tag{A3}$$

it possesses a temperature error. The mathematical operation, multiplying Equation (A2) by ρ_t/ρ_d and then subtracting Equation (A3), yields the expression for the error

$$\left(\frac{d\theta}{dt}\right)_{approx} \sim \theta\frac{dq_v}{dt}$$

with the aid of Equation (A1).

In cloudy air, q_v=q_{vs} the saturation mixing ratio of water vapor. Using the Clausius-Clapeyron equation and the hydrostatic balance approximation, the proceeding expression for the error is simplified into

$$\left(\frac{d\theta}{dt}\right)_{approx} \sim \theta q_{vs}\left(\frac{L_v\gamma_s}{R_v T^2} - \frac{g}{R_d T}\right)w \tag{A4}$$

where w is the vertical velocity, γ_s the temperature lapse rate of saturated air, L_v the latent heat of vaporization and R_v the gas constant of water vapor. Let $\theta \sim T \sim 273$ K, $q_{vs} \sim 5$ g/kg, and $\gamma_s \sim 0.6 \times 10^{-2}$ K/m. Thus $(d\theta/dt)_{approx} \sim 10^{-1}$ K/day when w=0.01 m/s. The error increases with the vertical velocity. When w=0.1 m/s, the error is 10^0 K/day, which is the order of the atmospheric radiative cooling rate.

Zeng, Tao and Simpson (2004) used the model of Neelin and Held (1987) to show the sensitivity of the large-scale vertical circulations to the atmospheric cooling rate in the Tropics. Their results indicated that the accumulative temperature error should be $\sim 10^{-1}$ K/day or less for the correct simulation of tropical large-scale vertical circulations. Hence the approximation in Equation (A3) should be avoided in the numerical simulation of tropical, large-scale circulations.

APPENDIX B

Fourier Stability Analysis

The computational stability of the compensation method is analyzed in this appendix. Similar to the system in Section 3, the following linear system is introduced

$$\partial_t w + \partial_z p = 0 \tag{B1a}$$

$$\partial_t \rho + \partial_z w = 0 \tag{B1b}$$

$$\partial_t p - c_s^2 \partial_t \rho + (p - c_s^2 \rho)/\tau_s = 0 \tag{B1c}$$

where (w, ρ, p) are prognostic variables, and (c_s, τ_s) are constants. It is discretized on three time levels as

$$w_j^{*n+1} = w_j^{n-1} - \frac{2\Delta t}{\Delta z}(p_{j+1/2}^n - p_{j-1/2}^n) \tag{B2a}$$

$$\rho_{j+1/2}^{n+1} = \rho_{j+1/2}^{n-1} - \frac{2\Delta t}{\Delta z}(w_{j+1}^n - w_j^n) \tag{B2b}$$

$$p_{j+1/2}^{*n+1} = p_{j+1/2}^{n-1} + c_s^2(\rho_{j+1/2}^{n+1} - \rho_{j+1/2}^{n-1}) + \frac{2\Delta t}{\tau_s}(p_{j+1/2}^{n-1} - c_s^2 \rho_{j+1/2}^{n-1}) \tag{B2c}$$

where Δt is the time step and Δz the spatial grid size; the variables w and ρ are spatially staggered; and the variables with an asterisk will be used to calculate their final values on the time level $n+1$. If the variables with an asterisk are treated as their final values, Equation (B2) is a traditional method where the time step is limited by c_s the sound wave speed.

To increase the time step for integration, the following reference system is introduced just as in Section 3

$$\partial_t w + \partial_z p = 0 \tag{B3a}$$

$$\partial_t \rho + \partial_z w = 0 \tag{B3b}$$

$$\partial_t p - c_{sr}^2 \partial_t \rho = 0 \tag{B3c}$$

where c_{sr} is the sound wave speed in the reference system. Equation (B3) uses the same finite-difference scheme as Equation (B2). After the different values of the variables on the time level n+1 in the two systems are obtained, the expressions for S_{cw} and S_{cp} in Equation (3.5) become

$$s_{cw(j)} = s_{cp(j+1/2)} = 0 \tag{B4a}$$

$$s_{cp(j+1/2)} = -(c_s^2 - c_{sr}^2)(w_{j+1}^n - w_j^n)/\Delta z + (p_{j+1/2}^{n-1} - c_s^2 \rho_{j+1/2}^{n-1})/\tau_s \tag{B4b}$$

From Equations (3.8) and (3.10), the final values of the variables on the time level n+1 are obtained. For the sake of convenience, it is assumed here that $\tau_s^{-1} = 0$ and

$$\Delta t = m\frac{\Delta z}{2c_{sr}} \tag{B5}$$

where m=1, 2, ... is an integer. With the use of Equations (B4) and (B5), w^{n+1} and p^{n+1} are expressed from Equations (3.8) and (3.10) as

$$\begin{aligned} w_j^{n+1} = {} & \frac{w_{j-m}^{n-1} + w_{j+m}^{n-1}}{2} - \frac{(p_{j+1/2+m}^{n-1} + p_{j-1/2+m}^{n-1}) - (p_{j+1/2-m}^{n-1} + p_{j-1/2-m}^{n-1})}{4c_{sr}} \\ & + (\frac{c_s^2}{c_{sr}^2} - 1)\frac{w_{j+m}^n + w_{j-m}^n - 2w_j^n}{2} \end{aligned} \tag{B6a}$$

$$\begin{aligned} p_{j+1/2}^{n+1} = {} & \frac{p_{j+1/2+m}^{n-1} + p_{j+1/2-m}^{n-1}}{2} - c_{sr}\frac{(w_{j+1+m}^{n-1} + w_{j+m}^{n-1}) - (w_{j+1-m}^{n-1} + w_{j-m}^{n-1})}{4} \\ & - c_{sr}(\frac{c_s^2}{c_{sr}^2} - 1)\frac{(w_{j+1+m}^n + w_{j+m}^n) - (w_{j+1-m}^n + w_{j-m}^n)}{4} \end{aligned} \tag{B6b}$$

Fourier stability analysis (e.g., Lomax *et al.* 2001) is applied to Equation (B6). Consider a harmonic $\exp(\alpha t + ikz)$ where k is real. Let $\sigma \equiv \exp(\alpha\Delta t)$. Thus $|\sigma| \le 1$ for numerical stability. Substitution of the harmonic into Equation (B6) yields

$$\begin{aligned} & (\sigma^2 - \cos(km\Delta z))^2 + \sigma(c_s^2 c_{sr}^{-2} - 1)(1 - \cos(km\Delta z))(\sigma^2 - \cos(km\Delta z)) \\ & + \cos^2(k\Delta z/2)\sin^2(km\Delta z)(1 - \sigma(c_s^2 c_{sr}^{-2} - 1)) = 0 \end{aligned} \tag{B7}$$

When c_{sr}=c_s, the expression for σ is obtained from Equation (B7), or

$$|\sigma|^4 = 1 - \sin^2(k\Delta z/2)\sin^2(km\Delta z) \tag{B8}$$

Thus $|\sigma| \leq 1$ which shows that the analytical solution is stable. All modes decay in time except for the modes with $\sin(km\Delta z) = 0$.

When $c_{sr} \neq c_s$ and $\sin(km\Delta z) = 0$, the expression for σ is obtained from Equation (B7), or

$$|\sigma| = 1 \tag{B9}$$

when $|c_s^2 c_{sr}^{-2} - 1| \leq 1$. Equation (B9) shows that the modes with $\sin(km\Delta z) = 0$ do not grow in time when $c_{sr} \neq c_s$.

APPENDIX C

A Numerical Scheme for Scalar Advection in the Compensation Method

A numerical scheme is introduced in this appendix for scalar advection under the discrete constraint. First the discrete air mass continuity equation in the compensation method is summarized. Then a scheme for scalar advection is proposed on the basis of the discrete air mass continuity equation.

In the compensation method, there is a discrete form of the air mass continuity equation

$$\frac{\rho_{j+1/2}^{*n+1}-\rho_{j+1/2}^{n-1}}{2\Delta t}+\frac{(\rho_{j+3/2}^{n}+\rho_{j+1/2}^{n})w_{j+1}^{n}-(\rho_{j+1/2}^{n}+\rho_{j-1/2}^{n})w_{j}^{n}}{2\Delta z}+\cdots=0 \quad \text{(C1)}$$

where Δz is the spatial grid size and the variables w and ρ are spatially staggered; the superscript n and the subscript j indicate time level and space grid-point, respectively; the air density $\rho_{j+1/2}^{*n+1}$, a temporary value, is different from the final value $\rho_{j+1/2}^{n+1}$ in the compensation method.

Since the time step Δt is large in the compensation method, the distance that sound waves travel in Δt is much larger than Δz. Thus the cloud-resolving model is computationally unstable if $\rho_{j+1/2}^{n+1}=\rho_{j+1/2}^{*n+1}$ is set. In other words, $\rho_{j+1/2}^{n+1}$ is determined by not only w_j^n and w_{j+1}^n but also the vertical velocity at other grid-points.

In the compensation method, $\rho_{j+1/2}^{n+1}$ is known at last. With reference to Equation (C1), $\rho_{j+1/2}^{n+1}$ is expressed using w_j^n and w_{j+1}^n in the following form

$$\frac{\rho_{j+1/2}^{n+1}-\rho_{j+1/2}^{n-1}}{2\Delta t}+\frac{(\rho_{j+3/2}^{n}+\rho_{j+1/2}^{n})(w_{j+1}^{n}+w_{j+1}^{(s)n})-(\rho_{j+1/2}^{n}+\rho_{j-1/2}^{n})(w_{j}^{n}+w_{j}^{(s)n})}{2\Delta z}+\cdots=0 \quad \text{(C2)}$$

where the equivalent velocity $w^{(s)}$ is introduced to explain $(\rho_{j+1/2}^{n+1} - \rho_{j+1/2}^{*n+1})$ the deviation of the final air density from the prediction of Equation (C1) at $2\Delta t$ due to sound waves. Subtracting Equation (C1) from (C2) yields

$$\frac{\rho_{j+1/2}^{n+1} - \rho_{j+1/2}^{*n+1}}{2\Delta t} + \frac{(\rho_{j+3/2}^{n} + \rho_{j+1/2}^{n}) w_{j+1}^{(s)n} - (\rho_{j+1/2}^{n} + \rho_{j-1/2}^{n}) w_{j}^{(s)n}}{2\Delta z} = 0 \qquad \text{(C3)}$$

which determines $w^{(s)n}$ with the aid of the boundary condition $w^{(s)n}=w^n$ at $z=0$ and z_{top}. Obviously $w^{(s)n}$ is much smaller than the phase speed of sound waves.

Once $w^{(s)n}$ is known, it is easy to construct a discrete form of the equation for scalar advection under the constraint. With reference to Equation (C2), Equation (2.4) can take the following discrete form

$$\frac{\rho_{j+1/2}^{n+1}\phi_{j+1/2}^{n+1} - \rho_{j+1/2}^{n-1}\phi_{j+1/2}^{n-1}}{2\Delta t} + \cdots +$$
$$\frac{(\rho_{j+3/2}^{n}\phi_{j+3/2}^{n} + \rho_{j+1/2}^{n}\phi_{j+1/2}^{n})(w_{j+1}^{n} + w_{j+1}^{(s)n}) - (\rho_{j+1/2}^{n}\phi_{j+1/2}^{n} + \rho_{j-1/2}^{n}\phi_{j-1/2}^{n})(w_{j}^{n} + w_{j}^{(s)n})}{2\Delta z} = 0 \qquad \text{(C4)}$$

When the scalar ϕ is constant, Equation (C4) reduces into Equation (C2). In other words, the scheme in Equations (C2) and (C4) complies with the discrete constraint, and Equation (C4) does not change scalar advection.

REFERENCES

Anderson, J. R., K. K. Droegemeier and R. B. Wilhelmson, 1985: Simulation of the thunderstorm subcloud environment. *Preprint 14th Conf. on Severe Local Storms*. Indianapolis, 147-150.

Arakawa, A, 2004: The cumulus parameterization problem: past, present, and future. Submitted to *J. Climate*.

Droegemeier, K. K. and R. B. Wilhelmson, 1987: Numerical simulation of thunderstorm outflow dynamics. Part I: Outflow sensitivity experiments and turbulence dynamics. *J. Atmos. Sci.*, **44**, 1182-1210.

Droegemeier, K. K., M. Xue, K. Johnson, M. O'Keefe, A. Sawdey, G. Sabot, S. Wholey, K. Mills and N.-T. Lin, 1995: Weather prediction: A scalable storm-scale model. *High Performance Computing*, Addison-Wesley, Reading, Massachusetts, 246 pp.

Grabowski, W. W., 1989: Numerical experiments on the dynamics of the cloud-environment interface: small cumulus in a shear-free environment. *J. Atmos. Sci.*, **46**, 3513-3541.

Lomax, H., T. H. Pulliam and D. W. Zingg, 2001, *Fundamentals of Computational Fluid Dynamics*. Springer-Verlag Berlin Heidelberg New York, 249pp.

Juang, H.-M. H., C.-H. Shiao and M.-D. Cheng, 2003: The Taiwan central weather bureau regional spectral model for seasonal prediction: multiparallel implementation and preliminary results. *Mon. Wea. Rev.*, **131**, 1832-1847.

Klemp, J. B. and R. B. Wilhelmson, 1978: The simulation of three-dimensional convective storm dynamics. *J. Atmos. Sci.*, **35**, 1070-1096.

Neelin, J. D. and I. M. Held, 1987: Modeling tropical convergence based on the moist static energy budget. *Mon. Wea. Rev.*, **115**, 3-12.

Ogura, Y. and A. Phillips, 1962: Scale analysis of deep and shallow convection in the atmosphere. *J. Atmos. Sci.*, **19**, 173-179.

Ooyama, K. V., 1990: A thermodynamic foundation for modeling the moist atmosphere. *J. Atmos. Sci.*, **47**, 2580-2593.

Ooyama, K. V., 2001: A dynamic and thermodynamic foundation for modeling the moist atmosphere with parameterized microphysics. *J. Atmos. Sci.*, **58**, 2073-2102.

Raymond, D. J., 1995: Regulation of moist convection over the west Pacific warm pool. *J. Atmos. Sci.*, **52**, 3945-3959.

Raymond, D. J., 2000: Thermodynamic control of tropical rainfall. *Quart. J. Roy. Meteor. Soc.*, **126**, 889-898.

Raymond, D. J. and A. M. Blyth, 1986: A stochastic mixing model for nonprecipitating cumulus clouds. *J. Atmos. Sci.*, **43**, 2708-2718.

Raymond, D. J. and X. Zeng, 2000: Instability and large scale circulations in a two-column model of the troposphere. *Quart. J. Royal Meteor. Soc.*, **126**, 3117-3135.

Robert, A. J., 1966: The integration of a low order spectral form of the primitive meteorological equations. *J. Meteor. Soc. Japan*, **44**, 237-245.

Satoh, M., 2002: Conservative scheme for the compressible nonhydrostatic models with the horizontally explicit and vertically implicit time integration scheme. *Mon. Wea. Rev.*, **130**, 1227-1245.

Skamarock, W. C. and J. B. Klemp, 1992: The stability of time-split numerical methods for the hydrostatic and the nonhydrostatic elastic equations. *Mon. Wea. Rev.*, **120**, 2109-2127.

Tao, W.-K. and J. Simpson, 1993: The Goddard Cumulus Ensemble model. Part I: Model description. *Terr. Atmos. Oceanic Sci.*, **4**, 19-54.

Tao, W.-K., J. Simpson, D. Baker, S. Braun, M.-D. Chou, B. Ferrier, D. Johnson, A. Khain, S. Lang, B. Lynn, C.-L. Shie, D. Starr, C.-H. Sui, Y. Wang and P. Wetzel, 2003: Microphysics, radiation and surface processes in the Goddard Cumulus Ensemble (GCE) model. *Meteor. Atmos. Phys.*, **82**, 97-137.

Tompkins, A. M. and G. C. Craig, 1998: Radiative-convective equilibrium in a three-dimensional cloud ensemble model. *Quart. J. Roy. Meteor. Soc.*, **124**, 2073-2098.

Xue, M., K. K. Droegemeier and V. Wong, 2000: The Advanced Regional Prediction System (ARPS) - A multi-scale nonhydrostatic atmospheric simulation and prediction model. Part I: Model dynamics and verification. *Meteor. Atmos. Phys.*, **75**, 161-193.

Zeng, X., 2001: *Ensemble simulation of tropical convection*. Ph.D. dissertation, New Mexico Tech. New Mexico Tech Library, 124pp.

Zeng, X., W.-K. Tao and J. Simpson, 2004: An equation for moist entropy in a precipitating and icy atmosphere. Submitted to *J. Atmos. Sci.*

Figure Captions

Figure 1 The vertical velocity at z=6 km changes with time in the two experiments with no sponge layer for sound waves. The results in the traditional and the compensation methods are shown in the upper and the lower panels, respectively.

Figure 2 the same as Figure 1 except that a sponge layer for sound waves is introduced.

Figure 3 The vertical velocity at z=6 km changes with time in two experiments. The thick and the thin lines show the results in the two experiments with the traditional and the compensation methods, respectively. In the experiment with the traditional method, Δt=0.01 s, and a sponge layer for sound waves is introduced. In the experiment with the compensation method, Δt=10 s, and no sponge layer for sound waves is used.

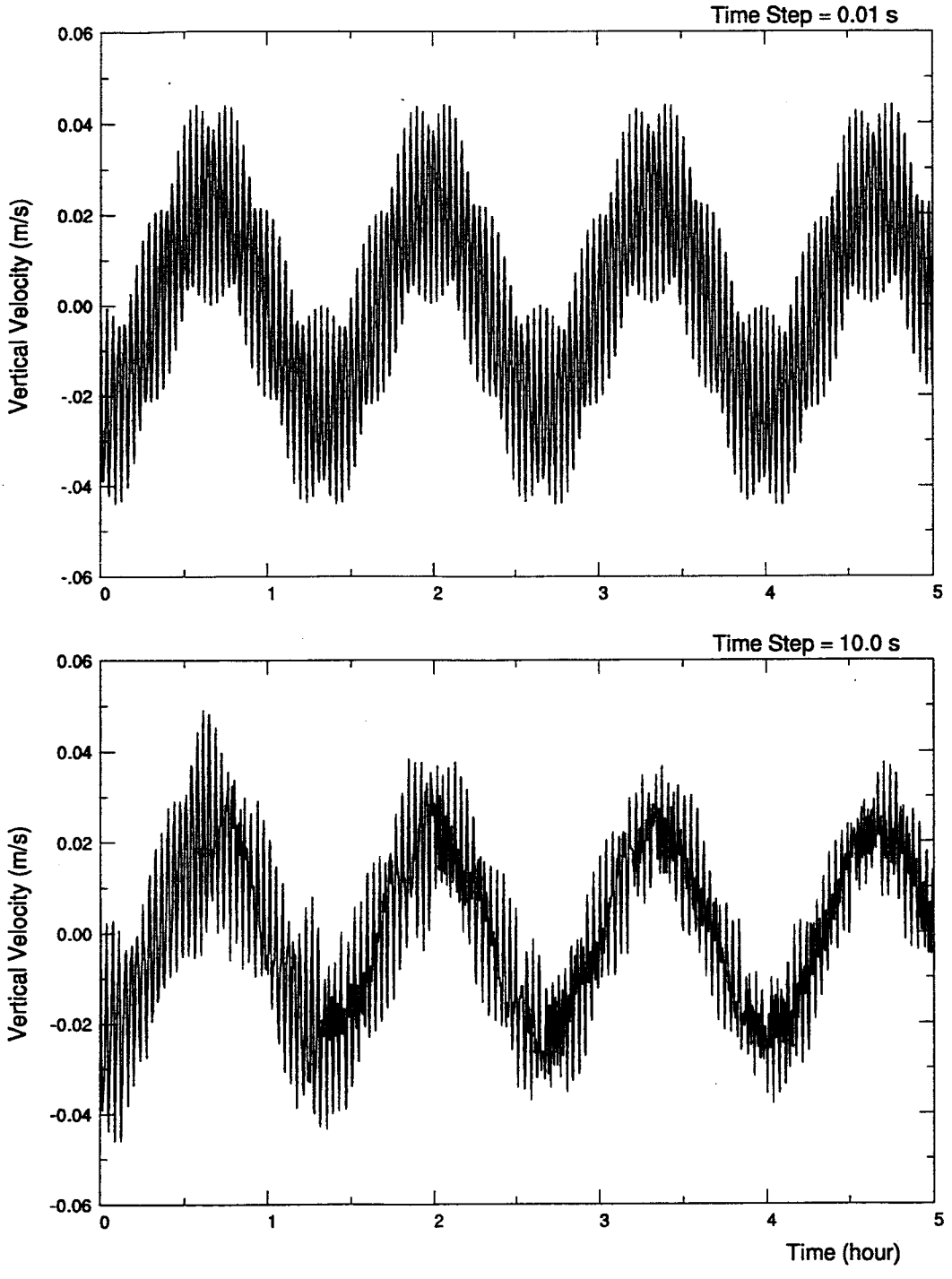

Figure 1 The vertical velocity at z=6 km changes with time in the two experiments with no sponge layer for sound waves. The results in the traditional and the compensation methods are shown in the upper and the lower panels, respectively.

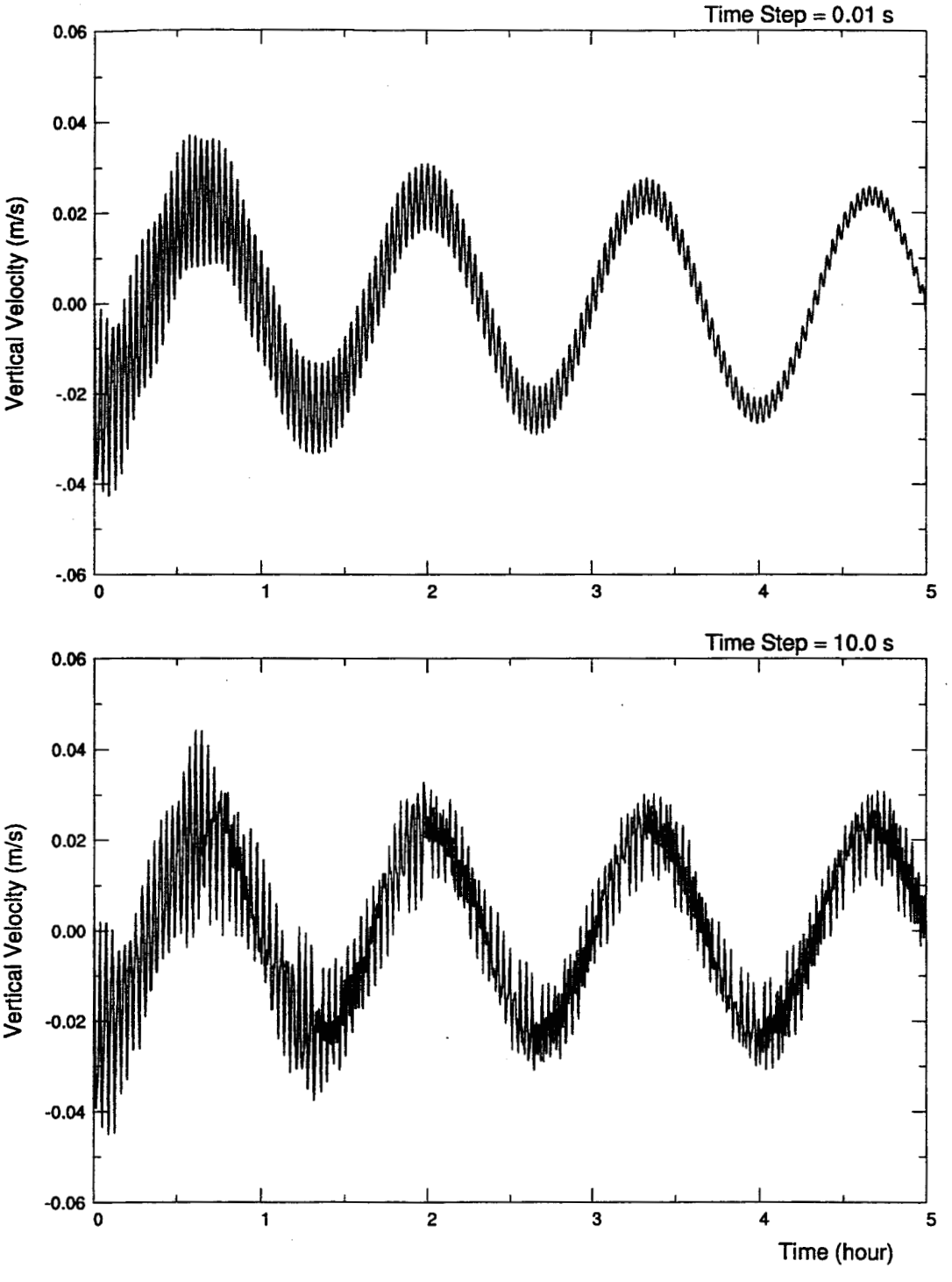

Figure 2 the same as Figure 1 except that a sponge layer for sound waves is introduced.

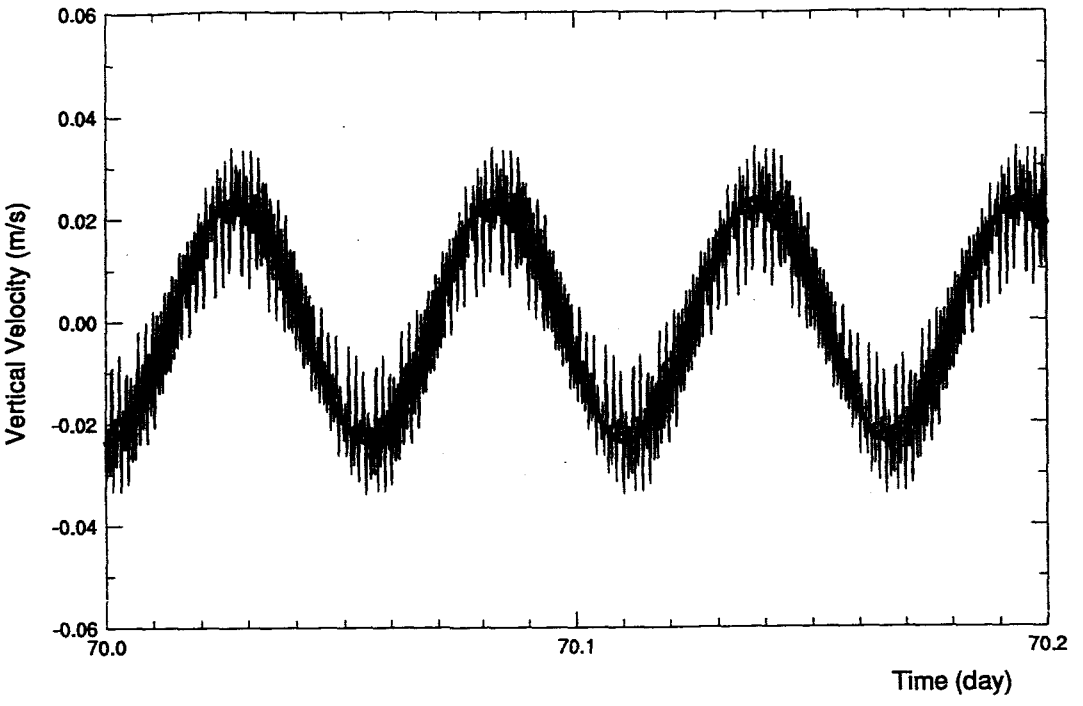

Figure 3 The vertical velocity at z=6 km changes with time in two experiments. The thick and the thin lines show the results in the two experiments with the traditional and the compensation methods, respectively. In the experiment with the traditional method, Δt=0.01 s, and a sponge layer for sound waves is introduced. In the experiment with the compensation method, Δt=10 s, and no sponge layer for sound waves is used.